DOI 10.1007/s11223-023-00581-w
Strength of Materials, Vol. 55, No. 5, September, 2023

EFFECT OF HYDROGEN ON THE STATIC CRACK RESISTANCE OF 05Kh13N8M3 CAST MARTENSITIC STEEL

O. I. Balytskyi[a,b,1] and L. M. Ivaskevych[a,2]

UDC 620.197:669.788

The laws governing the influence of a hydrogen atmosphere at a pressure of up to 15 MPa with controlled total oxygen and water vapor content of up to 0.004 g/m^3 and pre-absorbed hydrogen on the strength and ductility characteristics, short-term and long-term static crack resistance of 05Kh13N8M3 cast martensitic steel (in wt.%: 0.045 C, 0.38 Si, 12.9 Cr, 2.69 Mo, 0.43 Mn, 7.8 Ni, 0.057 La) at room temperature were studied. After hydrogen pre-charging for 4 h at a temperature of 773 K and a pressure of 5, 10, and 15 MPa, the hydrogen content of the specimens determined with a LECO TCH 600 device by infrared adsorption with melting was 3.3, 4.9, and 7.6 ppm, respectively. It was found that under short-term loading, the intensity of the effect of hydrogen on the fracture toughness of steel increases with an increase in the absorbed hydrogen content, crack sharpness, and a decrease in the loading rate. At the maximum hydrogen concentration of 7.6 ppm and a tensile rate of 0.1 mm/min, the relative elongation, lateral contraction ratio of smooth 25 mm long cylindrical specimens with a test portion diameter of 5 mm and the critical stress intensity factor of beam specimens measuring 20 × 10 × 100 mm with a relative length of the pre-induced crack of $\varepsilon = 0.53$ decrease almost twofold. At the same concentration, hydrogen does not affect the stress intensity factor of cracked specimens at a rate of 10 mm/min and specimens with a stress concentrator in the form of a notch with a tip radius of 0.065 mm at a rate of 0.1 mm/min. Under long-term static loading with a test duration of 300 h of double-cantilever beam specimens in the form of a rectangular plate 10 mm thick with milled grooves 3 mm deep and a tip angle of 60°, the threshold value of the stress intensity factor decreases. The rate of subcritical crack growth in the second portion of the hydrogen cracking diagram increases in proportion to the logarithm of hydrogen concentration.

***Keywords*:** martensitic steel, static crack resistance, hydrogen embrittlement, strength, ductility.

Introduction. Austenitic-martensitic stainless steels are used in the aerospace, thermal and nuclear power, automotive, medical equipment, and military industries [1–5]. By alloying and heat treatment of such materials, the percentage of strengthening phases, the ratio of austenite to martensite, and morphological types of martensite can be controlled, providing a combination of high mechanical properties, crack resistance, corrosion resistance, and wear resistance in the operating temperature range of –253 to 450°C following operational requirements [1–5]. The developed steels are not prone to the formation of hot crystallization cracks during casting and welding, making it possible to use them to manufacture pumps, gas generator parts, and geothermal turbine blades [1–3].

The development of hydrogen power engineering raises the issue of the performance of cast martensitic steels in the presence of hydrogen. Hydrogen embrittlement of wrought martensitic steels has been studied in many studies [6–9], while there is insufficient data on the effect of hydrogen on the properties of cast materials [10, 11]. A comparison of the mechanical characteristics of cast carbon steel, which had a pearlite, bainite, or martensitic structure after different heat treatment regimes, showed that the relative elongation of hydrogen-charged martensitic specimens

[a]Karpenko Institute of Physics and Mechanics of the Ukrainian National Academy of Sciences, Lviv, Ukraine ([1]balitskii@ipm.lviv.ua; [2]ivaskevich@ipm.lviv.ua). [b]West Pomeranian University of Technology in Szczecin, Szczecin, Poland. Translated from Problemy Mitsnosti, No. 5, pp. 39 – 48, September – October, 2023. Original article submitted July 18, 2023.

was only 2.88%. The fracture surface changed from a tough one with very small pits formed as a result of microcavity coalescence, typical for hydrogen-uncharged specimens, to a brittle transgranular one with some ductile areas in the central part of the specimen after hydrogen charging, indicating significant hydrogen embrittlement of the steel [11]. The hydrogen content of 1.6 mm thick flat martensitic steel specimens after electrolytic hydrogen charging was more than 10 ppm (total) and 4.7 ppm (diffusible). As a rule, large grain sizes, structure heterogeneity, and interfacial stresses characteristic of cast materials increase the sensitivity of materials to hydrogen [12–17]. Therefore, to assess the possibility of their use in hydrogen charging environments, it is necessary to determine the mechanical characteristics under such conditions experimentally.

Below are the results of studies of the effect of hydrogen atmosphere and pre-absorbed hydrogen on the short-term strength, ductility, and short-term and long-term static crack resistance of 05Kh13N8M3 cast martensitic steel.

Materials and Methods. 05Kh13N8M3 cast martensitic steel (0.045 C, 0.38 Si, 12.9 Cr, 2.69 Mo, 0.43 Mn, 7.8 Ni, 0.057 La wt.%) is used in gaseous hydrogen in the aerospace industry [18] for the manufacture of pumps and pipelines. After heat treatment (quenching from 1403 K, 3 h, cooling in air, double cold working at 220 K, 5 h, and tempering at 773 K, 3 h), it contains 75–90% packet (lath) martensite and 10–25% residual austenite, evenly distributed at the martensite boundaries in the form of layers 1–6 μm wide. The dimensions of the martensite packets are as follows: 30–100 × 90–250 μm, width of the laths 2–5 μm (Fig. 1). The carbides Me_2C and $Cr_{23}C_6$ are located at the boundaries and inside the grains.

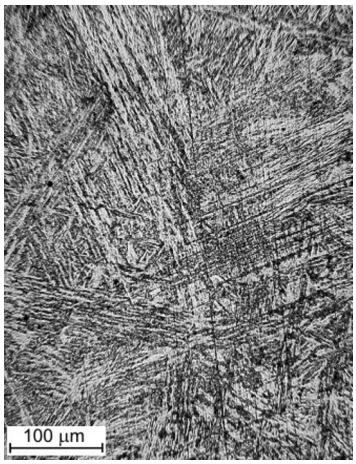

Fig. 1. Microstructure of 05Kh13N8M3 steel.

The study was conducted on four types of specimens (Table 1). For short-term tensile testing, ground 25 mm long cylindrical specimens with a test portion diameter of 5 mm were tested in air at a rate of 0.1 mm/min. The stress intensity factor (SIF) K_c under short-term loading of hydrogen-uncharged and hydrogen-precharged beam specimens measuring 10×20×100 mm was determined in the air according to the three-point bending scheme by the method [19–21] while recording force–time, force–COD diagrams at several points on the specimen surface using an analog-to-digital converter (ADC) and a computer. The values of K_c of the specimens with a stress concentrator in the form of a notch with a tip radius of 0.065 mm and the specimens with a pre-induced fatigue crack were compared. The relative lengths of the notch and fatigue crack are almost the same: $\varepsilon = 0.5$ and 0.53, respectively. Needle strain gauges were installed on the lateral surface of the specimen with a crack at distances a_1 and a_2 from its tip to measure the crack edge opening displacements W_1 and W_2 (Fig. 2).

According to the diagrams obtained (Fig. 3), the limiting value of the loading force P_c was set to calculate K_c. According to the limiting values of the force, the SIF was calculated from the formula [22, 23]:

$$K_c = \frac{P_c l}{t\sqrt{b^3}} Y(\varepsilon), \tag{1}$$

TABLE 1. Types and Dimensions of Specimens and Test Conditions

Specimen type	Test conditions	
	Hydrogen pre-charging conditions	Test environment
25 mm long cylindrical specimens with a test portion diameter of 5 mm	–	Air
	4 h at 773 K in hydrogen at 5, 10 and 15 MPa	Ditto
Beam specimens measuring 10×20×100 mm with a stress concentrator in the form of a notch with a tip radius of 0.065 mm	–	» »
	4 h at 773 K in hydrogen at 5, 10 and 15 MPa	» »
Beam specimens measuring 20x10x100 mm with a pre-induced fatigue crack with a relative length of $\varepsilon = 0.53$	–	» »
	4 h at 773 K in hydrogen at 5, 10 and 15 MPa	» »
Double-cantilever specimens in the form of a rectangular plate, size 25×10×100 mm	–	Hydrogen at a pressure of 10 MPa
	4 h at 773 K in hydrogen at 5, 10 and 15 MPa	

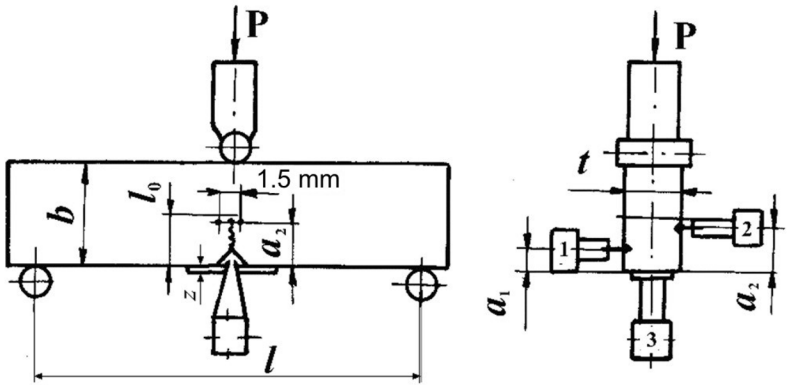

Fig. 2. Scheme for measuring the crack edges' displacements under a beam specimen's three-point bending.

where P_c is the ultimate loading force, l, t, and b are the geometric parameters of the specimen (Fig. 2), $Y(\varepsilon) = 3.494(1 - 3396(\varepsilon) + 5.839(\varepsilon)^2)$ is a coefficient that takes into account the geometry of the specimen.

Following the methodology of elastic-plastic fracture mechanics, to study the influence of the environment on crack growth [24, 25], the crack tip opening displacement was determined from the displacement of the crack edges measured by strain gauges at the distances a_1 and a_2 from the crack tip according to the empirical dependence:

$$\delta_c = W_1 \frac{a_2/a_1 - W_2/W_1}{a_2/a_1 - 1}, \tag{2}$$

where W_1 and W_2 are the displacement of the crack edges at different distances from the tip.

For comparison, the crack opening displacement was also calculated from a formula that takes into account the elastic and plastic components of crack edge displacements [25]:

$$\delta_c = \frac{K_1^2(1-\mu^2)}{2\sigma_Y E} + \frac{0.4(b-l)}{0.4b + 0.6l + z} W_3^p, \tag{3}$$

where σ_Y is the yield strength, E is Young's modulus, μ is Poisson's ratio, b and l are the geometric parameters of the specimen, z is the distance between the load line and the actual position of the strain gauge, and W_3^p is the plastic component of crack opening displacement.

TABLE 2. Effect of Hydrogen Content on the Mechanical Characteristics of Steel at 293 K at a Loading Rate of 0.1 mm/min

C_H, ppm	σ_u, MPa	$\sigma_{0.2}$, MPa	δ, %	ψ, %	K_c, MPa·m$^{1/2}$	K_c, MPa·m$^{1/2}$	δ_c, mm	δ_p, mm	K_{IHST}, MPa·m$^{1/2}$
					Stress concentrator	Fatigue crack			
0	1280	1110	20	63	190*	133*	0.300	0.082	–
3.3	1280	1100	18	42	186	103	0.241	0.079	29.8
4.9	1270	1090	16	38	184	84	0.177	0.076	25.9
7.6	1280	1100	13	33	182	69*	0.160	0.066	19.1

Note. The threshold value of the stress intensity factor K_{IHST} was determined in hydrogen at a pressure of 10 MPa. All other properties were determined in the air. The asterisk indicates the specimens whose tensile diagrams are shown in Fig. 3.

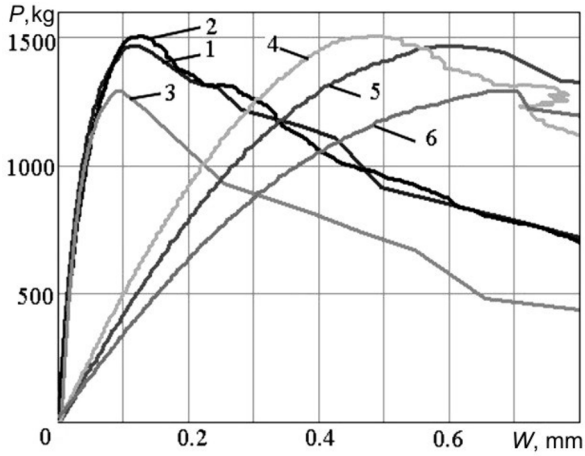

Fig. 3. Force–COD diagrams: (*1*, *4*) hydrogen-charged cracked specimen, (*2*, *5*) hydrogen-uncharged cracked specimen, (*3*, *6*) hydrogen-uncharged notched specimen [(*1*, *2*, *3*) crack tip opening displacement, (*4*, *5*, *6*) crack opening displacement on the surface]. The properties of the specimens are given in Table 2.

Using the above method, a series of specimens were tested in the air: hydrogen-uncharged specimens with a crack and a stress concentrator and hydrogen-charged specimens with a crack. The results of calculating crack tip and notch opening displacements and the CIF are given in Table 2.

To study the long-term crack resistance by the method [26], we used double-cantilever beam (DCB) specimens in the form of a rectangular plate with dimensions of 25×10×100 mm (Fig. 4). On both sides of the specimen, grooves were milled to a depth of 3 mm with a tip angle of 60°, and a through notch was milled at the end. Gradually, as the crack grew, the specimen was loaded using bolts that were screwed into threaded holes located perpendicular to the groove cross-section. The force was controlled by the number of revolutions of loading bolts and by the readings of a calibrated Bahco TAWM1430 digital torque wrench. The crack tip opening displacement, as well as the displacement along the axis of the bolts and from the end of the specimen, were measured by double-cantilever strain gauges calibrated with a micrometer. The signals from the strain gauge bridges were fed through amplifiers and a multichannel ADC to a computer, where they were stored in text files, which were used to construct plots of crack opening displacement versus time at the measurement points.

Some of the specimens were pre-incubated for 4 h at 773 K in hydrogen at 5, 10, and 15 MPa, and the absorbed hydrogen content of 10×10×10 mm witness specimens was measured with a Leko TCH 600 instrument. The hydrogen charging conditions ensure homogeneous hydrogen distribution over the specimen volume. The hydrogen embrittlement susceptibility of the alloy was estimated from the factor β, which was defined as the ratio of the values of the corresponding characteristics of specimens fractured in hydrogen and air.

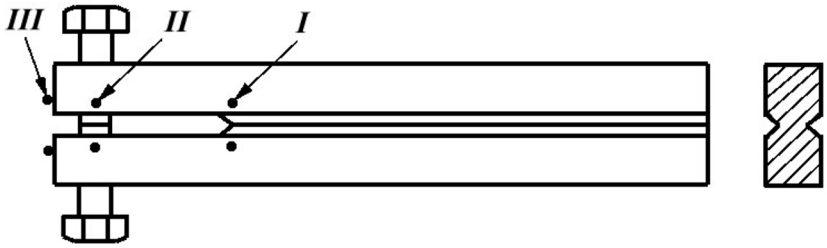

Fig. 4. Specimen for long-term crack resistance tests [(*I, II, III*) locations of the strain gauges for measuring crack opening displacement].

All tests were carried out at room temperature, using hydrogen with a controlled total oxygen and water vapor content of up to 0.004 g/m^3 after the double evacuation of the experimental chamber to a pressure of 0.13 Pa and intermediate hydrogen flushing.

Results and Discussion. It was found that during short-term tension in the air with an increase in the content of hydrogen pre-absorbed at 773 K, the ductility characteristics δ and ψ, the critical CIF K_c, and the crack opening displacement δ_c of the cracked specimens with the almost unchanged strength characteristics σ_u and $\sigma_{0.2}$ and the plastic component at the tip, δ_p, deteriorate significantly (Table 2, Fig. 5).

A comparison of the values of the SIF K_c of the specimens with a stress concentrator (notch radius 0.065 mm) and a fatigue crack showed that the crack resistance parameters of the specimens with a stress concentrator almost do not change with increasing hydrogen content (Fig. 5 curve *1*). In contrast, the specimens with a pre-induced crack are severely embrittled: K_c decreases at a hydrogen content of 7.6 ppm by half, i.e., just like the lateral contraction ratio of smooth cylindrical specimens (Fig. 5, curves *3* and *4*), which is one of the most sensitive characteristics of hydrogen embrittlement [9, 12–14, 22, 23, 27]. Similarly, the CIF K_c, the number of cycles to fracture, N, the relative elongation δ and the lateral contraction ψ of specimens of 03Kh12N10MT, 15Kh12N2MFAV, and 13Kh11N2V2MF martensitic steels [9] and 38KhN3MFA rotor steel [28] decrease intensively with an increase in external hydrogen pressure to 10 MPa. It should be noted that in static tensile tests, the lateral contraction ratio of cylindrical specimens with a diameter of 7 mm, a 1 mm deep notch, and a tip radius of 0.1 mm of 03Kh12N10MT steel and KhN51KVMTYuB nickel-cobalt alloy decreases threefold in gaseous hydrogen at a pressure of 35 MPa [29].

It is known that the degree of hydrogen-induced decrease in the ductility characteristics of wrought [9, 12-14, 22, 23, 28] and cast steels and the critical CIF of specimens of iron-nickel alloys [17, 23] and high-strength martensitic steels [25, 30] significantly depend on the strain rate. Therefore, we determined the CIF of hydrogen-charged (hydrogen concentration $C_{\mathrm{H}} = 7.6$ ppm) specimens with a fatigue crack at a 10 mm/min rate. In this case, $K_c = 132$ MPa·m$^{1/2}$, i.e., is almost equal to the value of K_c of hydrogen-uncharged specimens (Table 2). During short-term static tension at a rate of 10 mm/min, martensitic steels are significantly embrittled by hydrogen [9, 22], i.e., the fracture toughness in the presence of hydrogen is more sensitive to change in loading rate than the ductility characteristics.

Thus, under short-term loading, the influence of hydrogen on the critical CIF of 05Kh13N8M3 steel increases with an increase in absorbed hydrogen content, crack severity, and a decrease in loading rate.

It was found that during long-term static crack resistance tests with a test duration of 300 h, the hydrogen-uncharged specimens did not crack in hydrogen at a pressure of 10 MPa (Table 1). The diagrams of hydrogen cracking of hydrogen-precharged DCB specimens in hydrogen at a pressure of 10 MPa showed that in the first section of the diagram, the threshold value of the stress intensity factor K_{IHST} decreases in proportion to $\ln C_{\mathrm{H}}$ and in the second one, the rate of subcritical crack growth, V, increases, which is consistent with the known models based on the interaction between absorbed hydrogen and the stress field ahead of the crack [31, 32] (Fig. 6). Thus, at the stress intensity factor $K_{\mathrm{I}} = 40$ MPa·m$^{1/2}$, the rate changes from 4.1×10^{-6} (3.3 ppm) to 5.2×10^{-5} (7.6 ppm), see Fig. 7. The obtained values of K_c, V, and K_{IHST} can be used to calculate the durability and residual life of structural elements with cracklike defects in gaseous hydrogen.

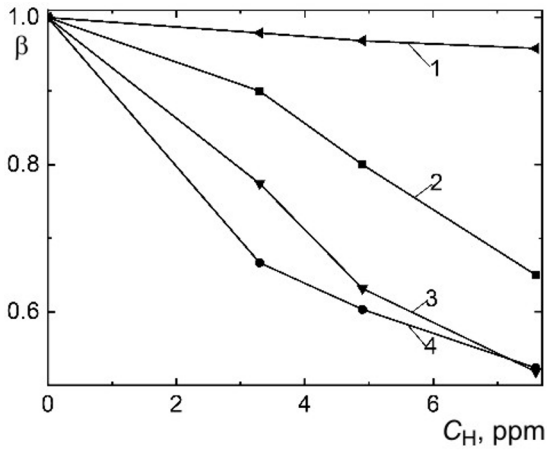

Fig. 5

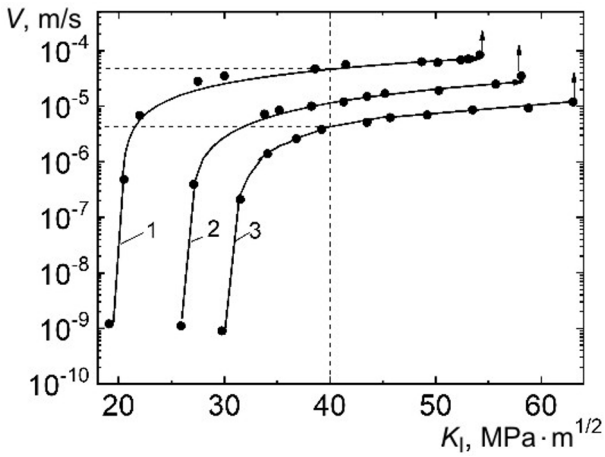

Fig. 6

Fig. 5. Dependence of the hydrogen influence factor β on the critical CIF K_c of specimens with a stress concentrator and a fatigue crack (*1*, *3*), relative elongation δ (*2*), and lateral contraction ψ (*4*) on the hydrogen content C_H at a tensile rate of 0.1 mm/min.

Fig. 6. Diagram of hydrogen cracking of hydrogen-charged DCB specimens at 293 K in hydrogen under a pressure of 10 MPa: (*1*) $C_H = 7.9$ ppm, (*2*) $C_H = 4.9$ ppm, and (*3*) $C_H = 3.3$ ppm. The test period is 300 h.

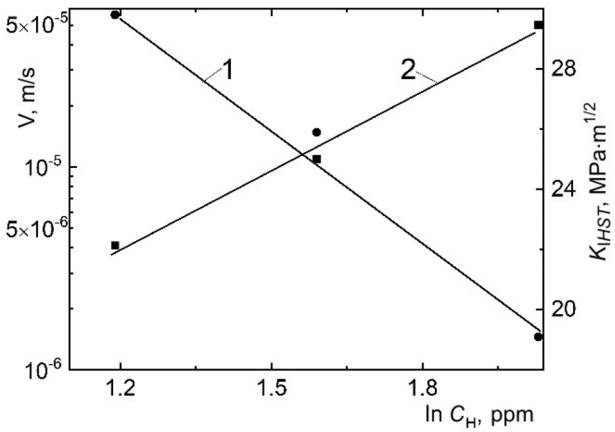

Fig. 7. Dependence of the threshold values of the critical SIF K_{IHST} (*1*) and the crack growth rate V at $K_I = 40$ MPa·m$^{1/2}$ (*2*) on the hydrogen content C_H.

CONCLUSIONS

1. During short-term static tension at a rate of 0.1 mm/min of smooth cylindrical and beam specimens of 05Kh13N8M3 cast martensitic steel with a pre-induced crack, the relative elongation δ, lateral contraction ratio ψ, critical stress intensity factor K_c, and crack opening displacement δ_c decrease significantly (almost twofold) with an increase in hydrogen content from 0 to 7.6 ppm. Hydrogen does not affect the values of K_c of cracked specimens at a rate of 10 mm/min and notched specimens with a tip radius of 0.065 mm at a rate of 0.1 mm/min.

2. Under the long-term static loading of double-cantilever beam specimens with a test duration of 300 h, the threshold value of the stress intensity factor K_{IHST} decreases, and the rate of subcritical crack growth, V, increases in proportion to the logarithm of the hydrogen content C_H.

The research was supported by the Ministry of Education and Science of Ukraine (contract M/34-2023) and the Polish National Agency for Academic Exchange (NAWA) (Grant number BPN/BUA/2021/1/00003/U/00001).

REFERENCES

1. R. Fan, M. Gao, Y. Ma, et al., “Effects of heat treatment and nitrogen on microstructure and mechanical properties of 1Cr12NiMo martensitic stainless steel,” *J Mater Sci Technol*, **28**, No. 11, 1059–1066 (2012). https://doi.org/10.1016/S1005-0302(12)60173-X
2. Y. Jin, T. Zhang, Q. Zang, et al., “Behavior of Nb influence on structure and properties of 30Cr13 cast martensitic stainless steel,” *J Iron Steel Res Int*, **26,** 462–471 (2018). https://doi.org/10.1007/s42243-018-0188-y
3. M. A. Prasetyo, V. Puspasari, M. S. Anwar, et al., “Mechanical properties of modified cast martensitic stainless steel CA6NM with addition of molybdenum and nitrogen,” in: Proc. of the 3rd Int. Seminar on Metallurgy and Materials (ISMM2019): Exploring New Innovation in Metallurgy and Materials (2020). https://doi.org/10.1063/5.0004773
4. A. Nagao, M. L. Martin, M. Dadfarnia, et al., “The effect of nanosized (Ti,Mo)C precipitates on hydrogen embrittlement of tempered lath martensitic steel,” *Acta Mater*, **74**, 244–254 (2014). https://doi.org/10.1016/j.actamat.2014.04.051
5. T. Tsuchiyama, J. Tobata, T. Tao, et al., “Quenching and partitioning treatment of a low-carbon martensitic stainless steel,” *Mater Sci Eng A*, **532**, 585–592 (2012). https://doi.org/10.1016/j.msea.2011.10.125
6. J. Lee, T. Lee, Y. J. Kwon, et al., “Effects of vanadium carbides on hydrogen embrittlement of tempered martensitic steel,” *Met Mater Int*, **22**, 364–372 (2016). https://doi.org/10.1007/s12540-016-5631-7
7. A. Shibata, T. Matsuoka, A. Ueno, et al., “Fracture surface topography analysis of the hydrogen-related fracture propagation process in martensitic steel,” *Int J Fracture*, **205**, 73–82 (2017). https://doi.org/10.1007/s10704-017-0182-6
8. Y. Momotani, A. Shibata, D. Terada, et al., “Effect of strain rate on hydrogen embrittlement in low-carbon martensitic steel,” *Int J Hydrogen Energy*, **42**, No. 5, 3371–3379 (2017). https://doi.org/10.1016/j.ijhydene.2016.09.188
9. O. I. Balyts’kyi, L. M. Ivas’kevich, and V. M. Mochulskyi, “Mechanical properties of martensitic steels in gaseous hydrogen,” *Strength Mater*, **44,** No 1, 64–71 (2012). https://doi.org/10.1007/s11223-012-9350-0
10. M. Pinson, L. Claeys, H. Springer, et al., “Investigation of the effect of carbon on the reversible hydrogen trapping behavior in lab-cast martensitic F-C steels,” *Mater. Charact*, **184**, 111671, 156–163 (2022). https://doi.org/10.1016/j.matchar.2021.111671
11. T. Depover, E. Wallaert, and K. Verbeken, “On the synergy of diffusible hydrogen content and hydrogen diffusivity in the mechanical degradation of laboratory cast Fe-C alloys,” *Mater Sci Eng A*, **664**, No. 10, 195–205 (2016). https://doi.org/10.1016/j.msea.2016.03.107
12. M. Dadfarnia, A. Nagao, S. Wang, et al., “Recent advances on hydrogen embrittlement of structural materials,” *Int J Fracture*, **196**, 223–243 (2015). https://doi.org/10.1007/ s10704-015-0068-4
13. M. Robertson, P. Sofronis, A. Nagao, et al., "Hydrogen embrittlement understood,” *Metall Mat Trans A*, **46**, 2323–2341 (2015). https://doi.org/10.1007/s11661-015-2836-1
14. R. P. Gangloff, “Science-based prognosis to manage structural alloy performance in hydrogen,” in: B. Somerday, P. Sofronis, and J. Russell (Eds.), *Effects of Hydrogen on Materials* (Proc. of the 2008 Int. Hydrogen Conference, Wyoming), ASM International, Materials Park, Geauga County, OH, USA (2009), pp. 1–21.
15. O. I. Balyts’kyi, Yu. H. Kvasnytska, L. M. Ivaskevych, et al., “Corrosion and hydrogen resistance of heatproof blade nickel-cobalt alloys,” *Mater Sci*, **54**, No. 2, 289–294 (2018). https://doi.org/ 10.1007/s11003-018-0178-z
16. I. M. Dmytrakh, A. M. Syrotyuk, and R. L. Leshchak, “Specific features of the deformation and fracture of low-alloy steels in hydrogen-containing media: Influence of hydrogen concentration in the metal,” *Mater Sci*, **54**, No. 3, 295–308 (2018). https://doi.org/10.1007/s11003-018-0186-z

17. I. Balitskii and L. M. Ivaskevich, “Hydrogen effect on cumulation of failure, mechanical properties, and fracture toughness of Ni-Cr alloys,” *Adv Mat Sci Eng*, **2019**, 3680253 (2019). https://doi.org/10.1155/2019/3680253
18. V. Fishgoit and B. A. Kolachev, “Strength tests in hydrogen in the aerospace industry,” *Mater Sci*, **33**, No. 4, 568–573 (1997). https://doi.org/10.1007/BF02537555
19. M. Syrotyuk and I. M. Dmytrakh, “Methods for the evaluation of fracture and strength of pipeline steels and structures under the action of working media. Part II. Influence of hydrogen-containing media,” *Mater Sci*, **50**, No. 4, 475–487 (2015). https://doi.org/10.1007/s11003-014-9724-5
20. V. V. Panasyuk, I. M. Dmytrakh, L. Toth, et al., “A method for the assessment of the serviceability and fracture hazard for structural elements with cracklike defects,” *Mater Sci*, **49**, No. 5, 565–576 (2014). https://doi.org/10.1007/s11003-014-9650-6
21. Y. L. Ivanyts’kyi, S. T. Shtayura, T. M. Lenkovs’kyi, et al., “Determination of the parameters of crack resistance for 17g1s steel under transverse shear,” *Mater Sci,* **49**, No 5, 637–643 (2014). https://doi.org/10.1007/s11003-014-9657-z
22. O. I. Balitskii and L. M. Ivaskevich, “Load rate-related mechanical properties of steels and alloys under static and cyclic loading in gaseous hydrogen,” *Strength Mater*, **53,** No. 3, 430–439 (2021). https://doi.org/10.1007/s11223-021-00303-0
23. O. I. Balyts’kyi, L. M. Ivas’kevych, and J. J. Eliasz, “Static crack resistance of heat-resistant KhN43MBTYu nickel-chromium alloy in gaseous hydrogen,” *Strength Mater*, **52**, No. 3, 386–397 (2020). https://doi.org/10.1007/s11223-020-00189-4
24. *BS 5762. Methods of Tests for Crack Opening Displacement Testing*, British Standards Institution (Gr. 6), London (1979).
25. W. Dietzel, “The use of crack-tip opening displacement for testing of the hydrogen embrittlement of high-strength steels,” *Mater Sci*, **40**, No. 6, 749–755 (2004). https:// doi.org/10.1007/s11003-005-0111-0
26. M. O. Speidel and M. V. Hyatt, “Stress-corrosion cracking of high-strength aluminum alloys,” *Adv Corros Sci Technol*, **2**, 115–335 (1972).
27. S. P. Lynch, “Mechanisms and kinetics of environmentally assisted cracking: current status, issues, and suggestions for further work,” *Metal Mat Trans A*, **44**, 1209–1229 (2013). https://doi.org/10.1007/s11661-012-1359-2
28. A. I. Balitskii, L. M. Ivaskevich, and O. A. Balitskii, “Rotor steels crack resistance and fracture behavior for hydrogen targeted materials ever-widening database,” *Eng Fract Mech*, **260**, 108168 (2022). https://doi.org/10.1016/j.engfracmech.2021.108168
29. V. I. Tkachov, L. M. Ivas’kevych, and O. M. Voznychak, “Degradation of steel in gaseous hydrogen with inhibiting admixtures,” *Mater Sci*, **43**, No. 3, 377–382 (2007). https://doi.org/10.1007/s11003-007-0043-y
30. H. Jia, X. Zhang, J. Xu, et al., “Effect of hydrogen content and strain rate on hydrogen-induced delay cracking for hot-stamped steel,” *Metals*, **9**, No. 7, 798 (2019). https:// doi.org/10.3390/met9070798
31. V. V. Panasyuk, A. E. Andreikiv, and O. I. Obukhivskii, “A calculation model of crack growth in metals under the action of hydrogen,” *Soviet Mater Sci*, **20**, No. 3, 199–202 (1984). https://doi.org/10.1007/BF00720906
32. O. E. Andreikiv and O. V. Hembara, “Propagation of cracks in metals under the action of hydrogen and long-term static loading,” *Mater Sci*, **41**, No. 3, 309–315 (2005). https://doi.org/ 10.1007/s11003-005-0167-x